

LSM-YOLO: A Compact and Effective ROI Detector for Medical Detection

Zhongwen Yu¹, Qiu Guan¹ (✉), Jianmin Yang², Zhiqiang Yang¹, Qianwei Zhou¹, Yang Chen³, and Feng Chen⁴

¹ College of Computer Science and Technology, Zhejiang University of Technology, Hangzhou, China

vincentyu67373@gmail.com
gq@zjut.edu.cn

² Zhejiang College of Sports, Hangzhou, China

³ SouthEast University, School of Computer Science and Engineering, Nanjing, China

⁴ The First Affiliated Hospital, Zhejiang University School of Medicine, Hangzhou, China

Abstract. In existing medical Region of Interest (ROI) detection, there lacks an algorithm that can simultaneously satisfy both real-time performance and accuracy, not meeting the growing demand for automatic detection in medicine. Although the basic YOLO framework ensures real-time detection due to its fast speed, it still faces challenges in maintaining precision concurrently. To alleviate the above problems, we propose a novel model named Lightweight Shunt Matching-YOLO (LSM-YOLO), with Lightweight Adaptive Extraction (LAE) and Multipath Shunt Feature Matching (MSFM). Firstly, by using LAE to refine feature extraction, the model can obtain more contextual information and high-resolution details from multiscale feature maps, thereby extracting detailed features of ROI in medical images while reducing the influence of noise. Secondly, MSFM is utilized to further refine the fusion of high-level semantic features and low-level visual features, enabling better fusion between ROI features and neighboring features, thereby improving the detection rate for better diagnostic assistance. Experimental results demonstrate that LSM-YOLO achieves 48.6% AP on a private dataset of pancreatic tumors, 65.1% AP on the BCCD blood cell detection public dataset, and 73.0% AP on the Br35h brain tumor detection public dataset. Our model achieves state-of-the-art performance with minimal parameter cost on the above three datasets. The source codes are at: <https://github.com/VincentYuuuuuu/LSM-YOLO>.

Keywords: Medical image detection · YOLO · Lightweight · Adaptive Feature Extraction · Multipath Feature Fusion.

1 Introduction

Medical imaging techniques such as Computed Tomography (CT) and Magnetic Resonance Imaging (MRI) are widely used in radiological examinations [16, 21].

The corresponding diagnoses, such as tumor screening and blood imaging analysis, which predominantly rely on senior doctors visually analyzing the images. There is a lack of tools and methods for automatic detection of Region of Interest (ROI) in medical images. Existing analyses based on medical imaging mostly focus on medical image segmentation, with few mature detection outcomes being applied in clinical practice. The sizes of lesions in medical imaging are not uniform, and lesions are difficult to detect in the early stages. Additionally, there is a scarcity of medical ROI detection models. What’s more, The small scale of medical datasets is not conducive to data-driven methods like deep learning. Therefore, our work hopes to expand in this field, combining automatic detection with medicine, aiming to provide a lightweight, easily deployable, efficient medical object detection model.

Nowadays, mainstream detectors fall into two categories: CNN-based, exemplified by YOLO [6, 7, 9, 15, 22–25], and Transformer-based, illustrated by DETR [2, 27, 29, 30]. The YOLO framework stands out for its remarkable balance between speed and accuracy, enabling fast and reliable object detection in images. Despite DETR’s excellent accuracy on large datasets like MS-COCO, its high computational cost and parameter count hamper its comprehensive performance, especially in specific sectors with smaller datasets, like medicine, where YOLO excels. It’s this superiority that motivates YOLO’s use in this work.

In medical imaging, the ROI for detection are relatively smaller, as lesions often only occur in certain parts of an organ in CT or MRI scans. And the relationship between the ROI and surrounding areas is crucial. How to properly handle the relationship between the two is an important issue. Typically, functions deployed on medical devices should be lightweight and should not consume too much resource, lowering operational costs while improving the quality of medical services. This is why we aim to achieve lightweight models.

To address the aforementioned challenges, we have developed a lightweight and easily deployable LSM-YOLO framework to contribute to medical image detection. Initially, we introduced the Receptive-Field Attention Convolutional operation (RFACnv) [28], utilizing a spatial attention mechanism to share convolutional kernel parameters. This means in the initial stages of feature extraction, the model learns the similarities and differences between the object area and its surroundings. To extract multi-scale feature maps, we designed the Lightweight Adaptive Extraction (LAE) to allow downsampling on the basis of retaining as much information-rich features as possible, which not only circumvents the issue of high computational demand associated with traditional convolutions but also dynamically extracts features during multi-scale sampling, allowing the model’s attention to focus more significantly on the object areas. After obtaining multi-scale feature maps, naturally, we provide a rational feature fusion mechanism—Multipath Shunt Feature Matching (MSFM). This allows the model to focus more on coordinates with greater weight values during the feature fusion process, thereby learning key information such as tumor characteristics and locations. Through the methods described above, we can obtain richer contextual and high-resolution information, which enhances the detection

accuracy and generalizability of the model. Furthermore, to address the issue of numerous small objects in medical imaging, we optimize the output head, specifically extending the Path Aggregation-Feature Pyramid Network (PA-FPN) [12] structure to improve detection capabilities for small objects, using four detection heads to complete the final output task.

2 Related Work

2.1 Medical ROI Detection

Medical ROI detection plays a crucial role in improving diagnosis accuracy, treatment planning, and surgical interventions. By automatically identifying and localizing targets of ROI, it helps radiologists and doctors in detecting early signs of diseases, such as cancer, enabling prompt intervention and better patient treatments.

Aiming at different organ regions, there are many works utilizing deep learning methods to achieve automatic medical ROI detection. Kang et al. [8] proposed RCS-YOLO to address the detection of brain tumors. Ahmed et al. [1] introduced the YOLO model into wrist abnormality detection. DeGPR [20] is a model focused on cell detection and counting, which can assist other object detectors. Huynh et al. [5] utilized object detection models for the automatic detection of acne skin diseases. CircleNet [13] is a model designed for detecting ball-shaped biomedical objects, such as glomeruli and cell nuclei, the author also proposes the use of circular bounding boxes for detecting spherical objects in medical tasks, aiming to better accommodate detection tasks with unique shapes. In the field of medical image processing, Shamshad et al. [18] conducted a comprehensive review of the various applications of Transformers, including classification, segmentation, detection, reconstruction, and registration. This systematic compilation is highly commendable.

2.2 Multi-scale Features for Object Detection

Introducing multi-scale features into object detection models is essential. Typically, larger features capture the textural details of smaller objects, while smaller features contain the semantic attributes of larger objects. Relying solely on single-scale features will omit detail information. For example, in an abdominal CT image, the size difference between the stomach and pancreas is significant. With only single-scale feature assistance, it is difficult for detectors to fully learn the unique features of the stomach and pancreas, possibly leading the model to recognize only the stomach without knowing what the pancreas looks like.

Balancing high-level semantic information with low-level visual information has always been a focus of numerous works. In this context, the Feature Pyramid Network (FPN) [11] structure has been widely adopted due to its method of cross-scale connection and fusion of multi-scale features. Subsequent work has optimized the FPN to further address the above issue. Path Aggregation Network (PAN) [12] enhances the integration of features at various levels through

a bottom-up pathway. Bidirectional Feature Pyramid Network (BiFPN) [19], a weighted bidirectional feature pyramid network, introduces learnable weights to apply multi-scale feature fusion from top to bottom and bottom to top repetitively. Unlike inter-layer interactions, Centralized Feature Pyramid (CFP) [14] focuses on intra-layer features to capture global long-distance dependencies. Additionally, Asymptotic Feature Pyramid Network (AFPN) [26] progresses to high-level features by fusing the low-level information of two adjacent layers, supporting interactions between non-adjacent layers. However, the introduction of multi-scale features into the model inevitably increases the computational cost. Deformable DETR [30] achieves a good fusion of multi-scale features at the expense of computational resources. Nevertheless, excessive information interchange might lead to the loss of low-level information and poses a challenge in balancing efficiency, accuracy, and lightweight design.

3 Methods

The architecture of the proposed LSM-YOLO network is shown in Fig.1. The network mainly extracts features in the backbone, integrates features in the head section, and combines with the four output heads to output.

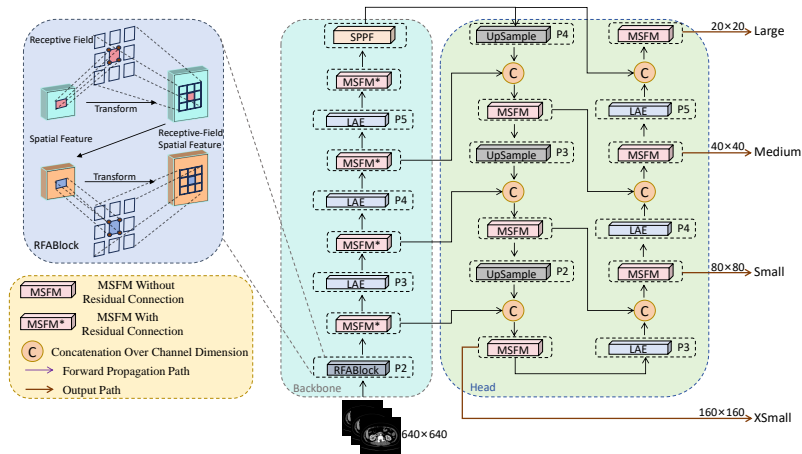


Fig. 1. Overview of the network architecture of LSM-YOLO. 1) LAE as a module to extract multi-scale feature maps; 2) MSFM as a module to refine and fuse high-level semantic and low-level spatial features.

3.1 Lightweight Adaptive Extraction

In multi-scale feature extraction, compared to the traditional convolution methods, LAE significantly reduces the number of parameters and computational

cost, while also extracting features with richer semantic information. Fig.2 shows the structural schematic diagram of LAE.

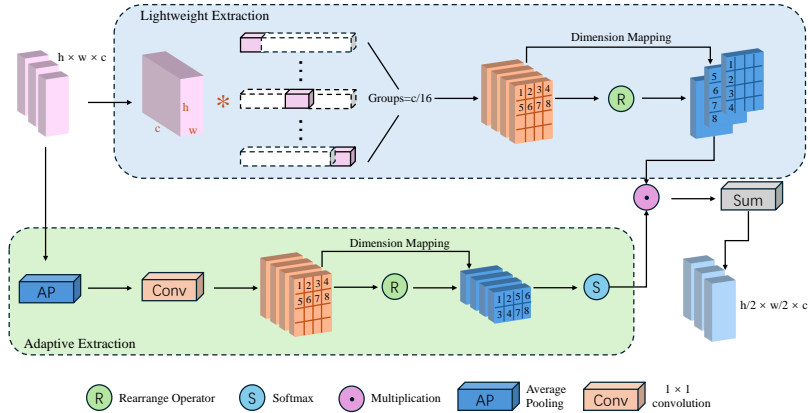


Fig. 2. The structure of Lightweight Adaptive Extraction (LAE) module.

In the process of traditional convolution, pixel information at the edges and corners is lost, but these local information is particularly important in medical imaging, as it represents the implicit information between the ROI targets and the surrounding areas. Additionally, there is a difference in information between adjacent pixels of the feature map, pixels containing the object have higher information entropy than their neighboring pixels, so we hope to preserve the pixels with higher information content during the sampling process.

Considering the local nature of convolution operations, difficult to capture global information while also involving complex computations. we referred to the concept of Focus [6], which uses slice operation to separate sampling by rows and columns. This achieves the aim of sampling while reducing information loss, essentially concentrating the feature map’s height and width information onto the channel level. However, we did not directly adopt the slice operation due to its high computational cost, which contradicts our goal of lightweight processing.

We designed two parallel branches with shared parameters, adopting the concept of group convolution to map the input to the output dimensions efficiently with low parameters. By utilizing group convolution with N groups, the number of parameters is reduced to $1/N$ compared to traditional convolution.

Each LAE unit achieves a four-fold downsampling, which means scaling both height and width by a factor of two. In order to alleviate the loss of edge information during sampling process, after saving feature map’s height and width information into channels, the feature map’s dimensions change from four-dimensional (batch, channel, height, weight) to five-dimensional (batch,

channel, height, weight, n), where 'n' represents the sampling factor. Adaptive Extraction path exchanges information via average pooling and convolution. Essentially, downsampling on this path recombines the feature map according to four adjacent pixels (such as the top left corner four pixels), with their respective weights expressed through softmax, also transforming the dimensions into five-dimensional. On 'n' dimension, adaptive weights are combined with the other branch. This method can be understood as implicitly including global information at the channel level during the transition from high-resolution to low-resolution information. Overall, the two branches are responsible for concentrating height and width information into the channels and calculating the corresponding information weights, respectively. Our LAE module is parameter-free when used, facilitating the plug-and-play transfer.

3.2 Multipath Shunt Feature Matching

In multi-scale feature fusion, we aim to break away from the traditional approach of relying solely on the interchange of channel information. This is because the multi-scale features extracted represent the mapping of objects of various sizes on the feature maps. Especially in medical imaging, such as tumor detection, the presence of a tumor is often associated with invasive phenomena and is characterized by multiple occurrences and a high tendency to metastasize. This is reflected in the feature map by a high degree of correlation in both the spatial and channel dimensions. The exchange of channel information can enhance the model's ability to capture visual information. However, a significant amount of semantic information is concentrated spatially, and the interaction of spatial information can assist in the detection of ROI with different scales. For instance, feature maps with low-resolution yet high semantic information are inherently used to predict larger targets. If we merge the high-level spatial information with the low-level visual information, it can have a complementary effect, using the global information from a larger receptive field to help the low-level feature maps predict smaller objects. Hence, our proposed MSFM module conducts a comprehensive analysis of spatial and channel information across features from low to high levels. Fig.3 shows the structural schematic diagram of MSFM.

The MSFM module follows the shunt concept, where the MatchNeck block is used to enhance the model's ability to represent ROI area features while controlling the number of parameters and computational complexity. The process starts by employing a split operator to divide the information flow, retaining the original features for subsequent residual connections. The MSFM module extracts information across the dimensions of height, width, and channels from the input feature tensor in a computationally efficient manner. Let average pooling and global average pooling operation be denoted as P_{avg} and P_{gavg} , the process of extracting F'_{out} from the input feature F_{in} is as follows:

$$F_h = P_{avg}(F_{in}^h), F_w = P_{avg}(F_{in}^w), F_c = P_{gavg}(F_{in}). \quad (1)$$

$$F'_{out} = Res(Align(F_h, F_w, F_c)). \quad (2)$$

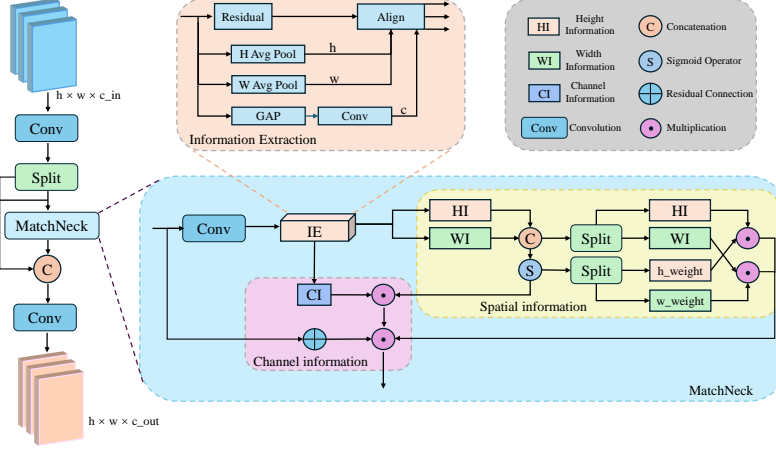


Fig. 3. The structure of Multipath Shunt Feature Matching (MSFM) module.

Incorporating height and width information into channels after normalization can help cascade global information, thereby capturing common features of ROI sites and their neighborhoods to promote the interaction of contextual information. Meanwhile, the spatial information stream integrated into the channel is preserved as auxiliary weights, which are then passed back to the spatial tensor through a multiplication operator. Let the height and width information after post-processing be \hat{F}_h and \hat{F}_w , with corresponding weights $weight_h$ and $weight_w$, the processing process of spatial information is as follows:

$$\hat{F}_h, \hat{F}_w = Split(Concat(F_h, F_w)). \quad (3)$$

$$weight_h, weight_w = Split(Sigmoid(Concat(F_h, F_w))). \quad (4)$$

Let the channel information after post-processing be \hat{F}_c , with the output as F_{out} , the process of the channel information branch is as follows:

$$\hat{F}_c = F_c \times Sigmoid(Concat(F_h, F_w)). \quad (5)$$

$$F_{out} = \hat{F}_c \times Res(F_{in}) \times \hat{F}_h * weight_h \times \hat{F}_w * weight_w. \quad (6)$$

After concatenating with the original source information and passing through a 1×1 convolution, the output is then produced.

MSFM module has two versions: one with residual connections and one without. In the backbone, we use the version with residual connections, as the primary task at this stage is to extract the main features of the object, providing meaningful feature representations for subsequent stages. The use of residual connections helps to mitigate the problem of vanishing gradients, thus accelerating the convergence of the model. In the head, we employ the version without residual connections. At this stage, the model has already extracted ample feature information, and the task is to analyze these features to predict objects. Therefore, residual connections become redundant here.

3.3 Loss Function

The loss function of LSM-YOLO is divided into a classification branch and a regression branch. The classification branch employs Binary Cross-Entropy Loss (BCE), while the regression branch is divided into Distribution Focal Loss (DFL) [10] and SCYLLA-IoU (SIoU) Loss [3]. The overall loss in this paper is a weighted combination of the above three, with each component being proportionally weighted. With $\gamma = 0.5$, $\zeta = 1.5$, $\eta = 7.5$, its definition is as follows:

$$Loss = \gamma BCELoss + \zeta DFL + \eta SIoULoss. \quad (7)$$

4 Experiments and Results

4.1 Datasets Details

To evaluate the proposed LSM-YOLO model, we use three different medical datasets. Our private CT pancreatic tumor dataset consists of serous cystic neoplasm and mucinous cystic neoplasm, with 1173 images in the training set and 309 images in the validation set. We use the MRI brain tumor dataset (Br35H) [4], which consists of a total of 701 images. Out of these, 500 images were used for training, and 201 images were used for validation. Additionally, we also utilize the Blood Cell Count and Detection (BCCD) [17] dataset, which includes 292 images in the training set and 72 images in the validation set.

4.2 Implementation Details

For model training and inference, we utilize two NVIDIA GeForce RTX 4090 GPUs. For YOLO-series models, we uniformly set the epoch to 300 and the input image size to 640×640 . For non-YOLO models, we conduct experiments with the epoch settings specified in their respective original papers. However, for RT-DETR, we set the epoch to 300 because we found that using the original paper’s [29] epoch of 72 did not lead to complete convergence on these datasets.

4.3 Results

We divide the comparison models into YOLO series and end-to-end DETR series, which are currently the two mainstream categories in object detection.

Tab.1 first compares proposed LSM-YOLO with YOLO-series detectors that are closest in size on the pancreatic tumor dataset. LSM-YOLO achieves fewer parameters and significantly higher accuracy. Further comparing it with larger models, LSM-YOLO still has a clear advantage on the pancreatic tumor dataset. In the comparison with DETR series models, the large number of parameters and computational load of the compared models did not result in positive gains. The reason is that the DETR series models lack the processing of multi-scale features, causing the deeper networks can not obtain sufficient ROI tumor features for predictions.

Table 1. Comparison with the state-of-the-art detectors on pancreatic tumor dataset.

Model	Params (M)	GFLOPs	AP _{50:95}	AP ₅₀	AP _S	AP _M	AP _L
YOLOv6-3.0-N	4.63	11.3	35.7	49.1	11.5	41.5	42.7
YOLOv7-T	6.01	13.0	34.7	48.4	12.5	45.1	35.1
YOLOv8-N	3.01	8.1	39.5	53.6	13.7	49.9	40.7
Gold-YOLO-N	5.60	12.1	32.7	44.7	9.3	38.1	45.7
YOLOv9-T	2.62	10.7	39.6	53.4	12.1	48.8	39.8
YOLOv10-N	2.70	8.2	38.3	51.7	12.0	47.3	38.0
YOLOv6-3.0-S	18.50	45.2	30.7	40.7	8.1	34.6	44.6
YOLOv7	36.49	103.2	32.5	44.0	18.1	40.0	32.1
YOLOv8-S	11.13	28.4	39.2	52.2	12.8	49.8	37.9
RCS-YOLO	45.70	94.5	35.9	47.6	10.1	45.7	35.7
Gold-YOLO-S	21.51	46.0	37.0	50.6	19.7	40.7	46.3
YOLOv9-S	9.60	38.7	39.9	52.8	13.0	50.9	36.9
YOLOv10-S	8.04	24.4	37.3	51.8	16.5	48.3	34.8
DINO-4scale-R50	46.60	179.4	27.2	36.8	7.7	50.6	42.4
DINO-5scale-R50	46.97	522.8	26.7	36.8	13.1	47.5	44.8
RT-DETR-R50	41.96	129.5	35.0	46.4	9.1	44.2	42.4
RT-DETR-HGNetv2-L	31.99	103.4	32.2	42.7	7.4	40.8	34.5
LSM-YOLO (ours)	2.87	12.4	48.6	60.8	21.9	51.1	54.5

Our proposed LSM-YOLO achieves 48.6% AP_{50:95} and 60.8% AP₅₀ on the pancreatic tumor dataset, outperforming the state-of-the-art detector among numerous detectors with lower parameter count and computational cost. LSM-YOLO has shown absolute superiority in small, medium and large objects detection.

We also experimented with larger-sized models, but the results indicated inferior performance compared to the smaller-sized models. From Tab.1, as the model size increases, the detection accuracy decreases. Therefore, it can be concluded that for smaller-scale medical datasets, smaller-sized models perform better.

Tab.2 compares our LSM-YOLO with other detectors on the BCCD blood cell dataset. Our LSM-YOLO achieves 65.1% AP_{50:95} and 92.7% AP₅₀, demonstrating state-of-the-art performance with relatively low parameter count and computational cost. It can be seen that on blood cell dataset, which is the dense multi-object detection task, the YOLO series models and the DETR series models perform similarly. The reason is that this type of dataset has a distribution where large targets are easy to detect but multiple overlapping targets are difficult to detect. Both types of models do not perform well in detecting the latter. However, our LSM-YOLO, due to its effective feature fusion mechanism, is sensitive to the regions surrounding the targets and better captures potential ROI area features, thus achieving a better detection rate. Compared with RT-

Table 2. Comparison with the state-of-the-art detectors on BCCD dataset.

Model	Params (M)	GFLOPs	AP _{50:95}	AP ₅₀	AP _S	AP _M	AP _L
YOLOv6-3.0-N	4.63	11.3	61.7	90.5	32.6	50.8	47.5
YOLOv7-T	6.01	13.0	61.8	91.8	31.7	51.2	47.4
YOLOv8-N	3.01	8.1	62.9	91.4	41.0	51.7	48.0
RCS-YOLO	45.71	94.5	59.8	89.4	42.3	46.2	45.7
Gold-YOLO-N	5.60	12.1	57.0	89.7	36.6	45.9	45.5
YOLOv9-T	2.62	10.7	63.0	92.2	34.8	51.8	48.1
YOLOv10-N	2.70	8.2	63.0	90.8	39.7	52.5	48.5
DINO-4scale-R50	46.60	236.1	56.8	83.4	45.1	43.4	44.2
DINO-5scale-R50	46.97	694.5	57.2	81.7	46.6	44.4	44.6
RT-DETR-R50	41.96	129.6	62.4	89.5	22.3	50.2	47.8
RT-DETR-HGNetv2-L	31.99	103.4	61.5	89.5	28.7	48.7	47.0
LSM-YOLO (ours)	2.87	12.4	65.1	92.7	41.1	53.4	49.7

DETR-R50, LSM-YOLO reduces the number of parameters by 93.2% and the computational amount by 90.4%, while significantly improves accuracy. Experimental results highlight that LSM-YOLO has a clear advantage in the overall AP metrics. While ensuring a high detection rate for easy-to-detect large targets, it also demonstrates excellent detection performance for small and medium targets with overlapping and coverage.

Tab.3 presents the comparison of our LSM-YOLO with other detectors on the Br35H brain tumor dataset. Our LSM-YOLO achieves 73.0% AP_{50:95}

Table 3. Comparison with the state-of-the-art detectors on Br35H dataset.

Model	Params (M)	GFLOPs	AP _{50:95}	AP ₅₀	AP _S	AP _M	AP _L
YOLOv6-3.0-N	4.63	11.3	70.7	93.2	27.6	71.4	74.5
YOLOv7-T	6.01	13.0	69.7	94.5	30.6	68.9	75.8
YOLOv8-N	3.01	8.1	70.0	93.6	20.7	70.6	73.5
RCS-YOLO	45.70	94.5	72.9	94.6	19.8	71.5	77.3
Gold-YOLO-N	5.60	12.1	70.3	93.8	24.7	71.3	73.7
YOLOv9-T	2.62	10.7	71.2	93.0	18.4	70.6	76.6
YOLOv10-N	2.70	8.2	69.3	91.6	20.5	68.7	72.3
DINO-4scale-R50	46.60	203.0	68.5	91.2	21.1	68.3	74.8
DINO-5scale-R50	46.97	593.8	69.7	91.9	18.2	70.8	74.7
RT-DETR-R50	41.96	129.5	72.1	94.1	27.4	70.9	75.7
RT-DETR-HGNetv2-L	31.99	103.4	71.8	93.0	29.3	69.9	76.0
LSM-YOLO (ours)	2.87	12.4	73.0	95.6	34.5	69.9	76.7

and 95.6% AP_{50} , outperforming the previous state-of-the-art model RCS-YOLO while significantly reducing parameter count and computational cost. This establishes LSM-YOLO as the new state-of-the-art model on this dataset.

From the AP metrics in Tab.3, LSM-YOLO has a significant advantage in detecting small tumors. This further demonstrates that for the ROI area, our model has effectively learned the contrast features between the target area and its surroundings, resulting in a higher recall rate. It proves that LSM-YOLO can leverage its performance advantages to better assist clinicians in diagnosis.

Based on the experimental results from the three datasets, our proposed LSM-YOLO demonstrates its adaptability to detection tasks across multiple organ ROI targets. Compared to the current popular YOLO-series detectors and DETR-series detectors, LSM-YOLO achieves state-of-the-art performance without imposing excessive computational costs. This has evident practical significance for clinical applications.

4.4 Visualization

To better demonstrate the detection performance, we use visualization of detection results and Class Activation Map (CAM) to intuitively display the ROI detection effect. In the visualization figures, the first row of sub-figures visualizes the detection results, while the second row represents class activation maps.

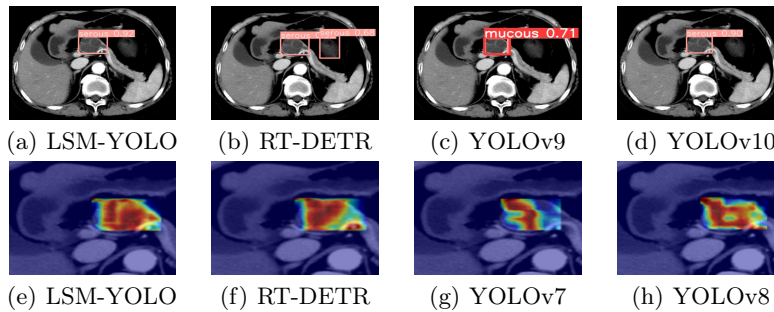


Fig. 4. Visual comparisons for tumor ROI detection on the pancreatic tumors dataset.

From Fig.4’s first row, Fig.4(a) shows LSM-YOLO successfully detecting the tumor location, achieving the highest confidence level of 0.92. Fig.4(b) illustrates a false detection case with RT-DETR, while Fig.4(c) shows that YOLOv9 misclassified the target. In Fig.4’s second row, it can be observed that LSM-YOLO exhibits the best activation effect compared to other detectors. Additionally, it is evident that our LSM-YOLO successfully detects a small portion derived from the right side of the tumor, which other detectors failed to detect.

The upper half of Fig.5 shows that LSM-YOLO can accurately detect overlapping cells and performs well in dense scenes, a result other detectors cannot achieve. In the class activation maps, LSM-YOLO’s activation effect on

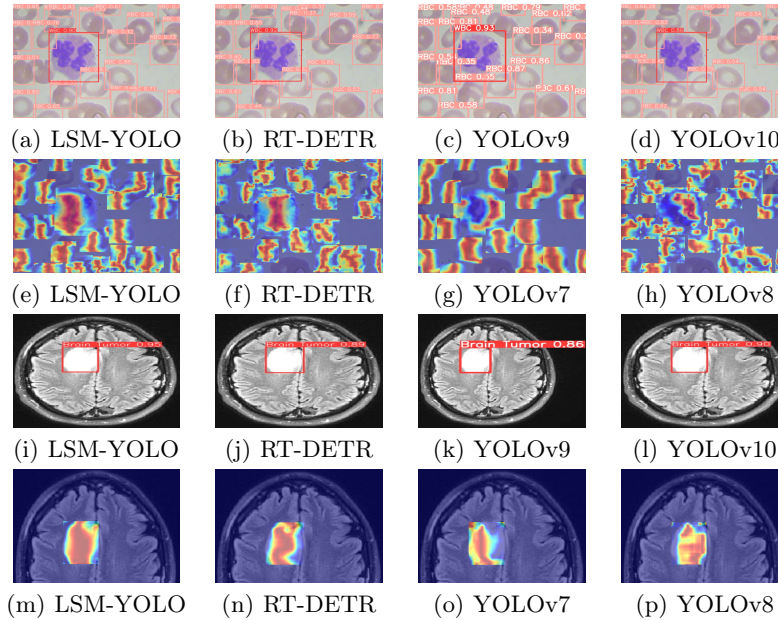


Fig. 5. Visual comparisons for cell ROI detection on the BCCD blood cell dataset (upper part) and Br35H brain tumor dataset (lower part).

incomplete cells at the edges is significantly better than that of other detectors.

From the lower half of Fig.5, it can be observed that LSM-YOLO has the highest confidence in correctly classifying brain tumor, and the activation area of the class activation map is the largest. This indicates that LSM-YOLO has the most comprehensive learning of tumor ROI features.

4.5 Ablation Study

In order to evaluate the effectiveness of proposed RFABlock, LAE, and MSFM modules, we conduct ablation experiments. As shown in Tab.4, compared to the experiment without these three modules, the addition of RFABlock, LAE, MSFM each improves the detection accuracy respectively. Furthermore, by incorporating the LAE and MSFM modules separately, the experimental results demonstrate that these two modules further enhance the detection performance. Finally, by incorporating all three modules, we obtain the optimal results.

As shown in Tab.5, we conduct ablation experiments on the internal modules Lightweight Extraction (LE) and Adaptive Extraction (AE) of LAE module, which respectively correspond to the upper and lower parts of Fig.2, and the Dimension Mapping (DM) module. In the experiments without LE, convolution is used for replacement. Incorporating LE and AE into the LAE module enhances the detection rate, with further improvement through DM integration and optimization. This proves the rationality of the internal modules within LAE.

Table 4. Ablation study on proposed RFABlock, LAE, and MSFM modules on the pancreatic tumor dataset.

RFABlock	LAE	MSFM	AP _{50:95}	AP ₅₀
			40.3	55.0
✓			42.1	58.1
	✓		42.7	57.6
		✓	43.6	55.5
✓		✓	43.9	57.6
✓	✓		45.3	58.3
✓	✓	✓	48.6	60.8

Table 5. Ablation study on internal modules of LAE on the pancreatic tumor dataset.

LE	AE	DM	AP _{50:95}	AP ₅₀
			43.7	55.0
✓			45.3	56.9
	✓		45.1	57.5
	✓	✓	46.6	59.0
✓	✓	✓	48.6	60.8

Table 6. Ablation study on internal modules of MSFM on the pancreatic tumor dataset.

Spatial	Channel	AP _{50:95}	AP ₅₀
		44.8	56.5
✓		46.7	57.2
	✓	46.3	57.7
✓	✓	48.6	60.8

Tab.6 displays the ablation experiments of the Spatial and Channel parts within the MSFM, where each part represents the refined fusion of features in different dimensions, which is beneficial for the interaction within the ROI areas and their neighborhoods in medical images. The AP_{50:95} metric improved from 44.8% to 48.6%, proving the effectiveness of the two internal components.

5 Conclusion

In this paper, we propose the LSM-YOLO network for lightweight and accurate medical ROI detection, which innovatively enhances feature extraction and fusion capabilities, especially in the detection of small targets in medical images, through the combination of LAE and MSFM modules. Additionally, the RFABlock is used to expand the receptive field by introducing the attention mechanism into the convolution process. Compared to other object detectors, LSM-YOLO demonstrates superior performance in evaluations on pancreatic tumor datasets, blood cell datasets, and brain tumor datasets, while having a low number of parameters and computational costs, proving its generalization ability and practicality in different medical image detection tasks, suitable for real-time medical image processing. At the same time, we find and verify in experiments that for small-scale medical imaging datasets, large-sized models do

not perform as well as small-sized models. In the future, we will continue to explore reliable medical image detectors to assist in clinical diagnosis.

Acknowledgments. This work is supported in part by National Natural Science Foundation of China (U20A20171, 62373324, 62271448), Natural Science Foundation of Zhejiang Province (LY21F020027) and Key Programs for Science and Technology Development of Zhejiang Province (2022C03113).

References

1. Ahmed, A., Imran, A.S., Manaf, A., Kastrati, Z., Daudpota, S.M.: Enhancing wrist abnormality detection with yolo: Analysis of state-of-the-art single-stage detection models. *Biomedical Signal Processing and Control* **93**, 106144 (2024)
2. Carion, N., Massa, F., Synnaeve, G., Usunier, N., Kirillov, A., Zagoruyko, S.: End-to-end object detection with transformers. In: *European conference on computer vision*. pp. 213–229. Springer (2020)
3. Gevorgyan, Z.: Siou loss: More powerful learning for bounding box regression. *arXiv preprint arXiv:2205.12740* (2022)
4. Hamada, A.: Br35h:: brain tumor detection 2020. kaggle (2020), <https://www.kaggle.com/datasets/ahmedhamada0/brain-tumor-detection>
5. Huynh, Q.T., Nguyen, P.H., Le, H.X., Ngo, L.T., Trinh, N.T., Tran, M.T.T., Nguyen, H.T., Vu, N.T., Nguyen, A.T., Suda, K., et al.: Automatic acne object detection and acne severity grading using smartphone images and artificial intelligence. *Diagnostics* **12**(8), 1879 (2022)
6. Jocher, G.: Yolov5 release v7.0 (2022), <https://github.com/ultralytics/yolov5/releases/tag/v7.0>
7. Jocher, G.: Yolov8 release v8.1.0 (2024), <https://github.com/ultralytics/ultralytics/releases/tag/v8.1.0>
8. Kang, M., Ting, C.M., Ting, F.F., Phan, R.C.W.: Rcs-yolo: A fast and high-accuracy object detector for brain tumor detection. In: *International Conference on Medical Image Computing and Computer-Assisted Intervention*. pp. 600–610. Springer (2023)
9. Li, C., Li, L., Jiang, H., Weng, K., Geng, Y., Li, L., Ke, Z., Li, Q., Cheng, M., Nie, W., et al.: Yolov6: A single-stage object detection framework for industrial applications. *arXiv preprint arXiv:2209.02976* (2022)
10. Li, X., Wang, W., Wu, L., Chen, S., Hu, X., Li, J., Tang, J., Yang, J.: Generalized focal loss: Learning qualified and distributed bounding boxes for dense object detection. *Advances in Neural Information Processing Systems* **33**, 21002–21012 (2020)
11. Lin, T.Y., Dollár, P., Girshick, R., He, K., Hariharan, B., Belongie, S.: Feature pyramid networks for object detection. In: *Proceedings of the IEEE conference on computer vision and pattern recognition*. pp. 2117–2125 (2017)
12. Liu, S., Qi, L., Qin, H., Shi, J., Jia, J.: Path aggregation network for instance segmentation. In: *Proceedings of the IEEE conference on computer vision and pattern recognition*. pp. 8759–8768 (2018)
13. Nguyen, E.H., Yang, H., Deng, R., Lu, Y., Zhu, Z., Roland, J.T., Lu, L., Landman, B.A., Fogo, A.B., Huo, Y.: Circle representation for medical object detection. *IEEE transactions on medical imaging* **41**(3), 746–754 (2021)

14. Quan, Y., Zhang, D., Zhang, L., Tang, J.: Centralized feature pyramid for object detection. *IEEE Transactions on Image Processing* (2023)
15. Redmon, J., Divvala, S., Girshick, R., Farhadi, A.: You only look once: Unified, real-time object detection. In: *Proceedings of the IEEE conference on computer vision and pattern recognition*. pp. 779–788 (2016)
16. Rydberg, J., Buckwalter, K.A., Caldemeyer, K.S., Phillips, M.D., Conces Jr, D.J., Aisen, A.M., Persohn, S.A., Kopecky, K.K.: Multisection ct: scanning techniques and clinical applications. *Radiographics* **20**(6), 1787–1806 (2000)
17. S., C.: Bccd (blood cell count and detection) dataset (2019), https://github.com/Shenggan/BCCD_Dataset
18. Shamshad, F., Khan, S., Zamir, S.W., Khan, M.H., Hayat, M., Khan, F.S., Fu, H.: Transformers in medical imaging: A survey. *Medical Image Analysis* p. 102802 (2023)
19. Tan, M., Pang, R., Le, Q.V.: Efficientdet: Scalable and efficient object detection. In: *Proceedings of the IEEE/CVF conference on computer vision and pattern recognition*. pp. 10781–10790 (2020)
20. Tyagi, A.K., Mohapatra, C., Das, P., Makharia, G., Mehra, L., AP, P., et al.: Degpr: Deep guided posterior regularization for multi-class cell detection and counting. In: *Proceedings of the IEEE/CVF Conference on Computer Vision and Pattern Recognition*. pp. 23913–23923 (2023)
21. Viallon, M., Cuvinciuc, V., Delattre, B., Merlini, L., Barnaure-Nachbar, I., Tosopatel, S., Becker, M., Lovblad, K.O., Haller, S.: State-of-the-art mri techniques in neuroradiology: principles, pitfalls, and clinical applications. *Neuroradiology* **57**, 441–467 (2015)
22. Wang, A., Chen, H., Liu, L., Chen, K., Lin, Z., Han, J., Ding, G.: Yolov10: Real-time end-to-end object detection. *arXiv preprint arXiv:2405.14458* (2024)
23. Wang, C., He, W., Nie, Y., Guo, J., Liu, C., Wang, Y., Han, K.: Gold-yolo: Efficient object detector via gather-and-distribute mechanism. *Advances in Neural Information Processing Systems* **36** (2024)
24. Wang, C.Y., Bochkovskiy, A., Liao, H.Y.M.: Yolov7: Trainable bag-of-freebies sets new state-of-the-art for real-time object detectors. In: *Proceedings of the IEEE/CVF conference on computer vision and pattern recognition*. pp. 7464–7475 (2023)
25. Wang, C.Y., Yeh, I.H., Liao, H.Y.M.: Yolov9: Learning what you want to learn using programmable gradient information. *arXiv preprint arXiv:2402.13616* (2024)
26. Yang, G., Lei, J., Zhu, Z., Cheng, S., Feng, Z., Liang, R.: Afpn: asymptotic feature pyramid network for object detection. In: *2023 IEEE International Conference on Systems, Man, and Cybernetics (SMC)*. pp. 2184–2189. IEEE (2023)
27. Zhang, H., Li, F., Liu, S., Zhang, L., Su, H., Zhu, J., Ni, L.M., Shum, H.Y.: Dino: Detr with improved denoising anchor boxes for end-to-end object detection. *arXiv preprint arXiv:2203.03605* (2022)
28. Zhang, X., Liu, C., Yang, D., Song, T., Ye, Y., Li, K., Song, Y.: Rfaconv: Innovating spatital attention and standard convolutional operation. *arXiv preprint arXiv:2304.03198* (2023)
29. Zhao, Y., Lv, W., Xu, S., Wei, J., Wang, G., Dang, Q., Liu, Y., Chen, J.: Detsr beat yolos on real-time object detection. *arXiv preprint arXiv:2304.08069* (2023)
30. Zhu, X., Su, W., Lu, L., Li, B., Wang, X., Dai, J.: Deformable detr: Deformable transformers for end-to-end object detection. *arXiv preprint arXiv:2010.04159* (2020)